ELSEVIER

Journal of Molecular Catalysis A: Chemical 180 (2002) 245–258

JOURNAL OF MOLECULAR CATALYSIS A: CHEMICAL

www.elsevier.com/locate/molcata

Relationship between the molybdenum phases and the conversion of *n*-butane over Mo/HZSM-5

Shandong Yuan [a], Sharifah Bee Derouane-Abd Hamid [b,1], Yongxue Li [b], Pinliang Ying [a], Qin Xin [a], Eric G. Derouane [b], Can Li [a,*]

[a] *State Key Laboratory of Catalysis, Dalian Institute of Chemical Physics, Chinese Academy of Sciences, P.O. Box 110, Dalian 116023, China*

[b] *Leverhulme Centre for Innovative Catalysis, Department of Chemistry, University of Liverpool, P.O. Box 147, Liverpool L69 3BX, UK*

Received 29 June 2001; accepted 8 November 2001

Abstract

The conversion of *n*-C_4H_{10} was undertaken on MoO_3/HZSM-5 catalyst at 773–973 K and the phases of molybdenum species were detected by XRD. The XRD results show that bulk MoO_3 on HZSM-5 can be readily reduced by *n*-C_4H_{10} to MoO_2 at 773 K and MoO_2 can be gradually carburized to molybdenum carbide above 813 K. The molybdenum carbide formed from the carburization of MoO_2 with *n*-C_4H_{10} below 893 K is α-MoC_{1-x} with fcc-structure, while hcp-molybdenum carbide formed above 933 K. During the evolution of MoO_3 to MoO_2 (>773 K) or the carburization of MoO_2 to molybdenum carbide (>813 K), deep oxidation, cracking and coke deposition are serious, in particular at higher reaction temperatures, these lead to the poor selectivity to aromatics. Aromatization of *n*-C_4H_{10} can proceed catalytically on both Mo_2C/HZSM-5 and MoO_2/HZSM-5, the distribution of the products for the two catalysts is similar below 813 K, but the activity for Mo_2C/HZSM-5 is much higher than that for MoO_2/HZSM-5.

Keywords: *n*-C_4H_{10}; Mo/HZSM-5; Molybdenum carbide; MoO_3; Aromatization

1. Introduction

Butane is one of the important building blocks for many chemicals, its catalytic upgrading has been extensively studied, e.g. dehydrogenation to butylene or butadiene [1–5], isomerization to *i*-butane [6–10], dehydro-isomerization by one-step to *i*-butylene [11–17], aromatization [18–22], etc. Most of these reactions can be catalysed effectively by bifunctional catalysts with acid sites and dehydrogenation sites. Zeolites containing 10-membered-ring, e.g. ZSM-5, ZSM-22 and MCM-22, are often chosen as the acidic materials due to their good resistance to coke deactivation. Noble metals are one of the most efficient dehydrogenation components for the upgrading of *n*-C_4H_{10}.

Since the 1970s, the similarities in the properties between noble metals and transition metal carbides have been continuously demonstrated. Carbides are also found to be active for dehydrogenation, hydrogenation, isomerisition, hydrocracking and some reactions typically catalysed by noble metals [23–29]. So carbide supported on HZSM-5 are expected to

* Corresponding author. Tel.: +86-411-4671991-728; fax: +86-411-4694447.
E-mail address: canli@ms.dicp.ac.cn (C. Li).
homepage: http://www.canli.dicp.ac.cn
[1] Present address: Chemistry Department, Faculty of Science, University Malaya, 50603 Kuala Lumpur, Malaysia, E-mail address: h1bee@umcsd.um.edu.my

1381-1169/02/$ – see front matter
PII: S1381-1169(01)00441-1

be able to catalyse the upgrading of n-C_4H_{10}. In the present work, we selected the aromatization of n-C_4H_{10} as the model reaction.

For the aromatization of n-C_4H_{10}, many components supported on HZSM-5 have been tested, e.g. Pt, Mo, Cr, Cu, V, Ni, Ga, In, Zn, etc. [18–22,30–37]. The preferred catalysts are Zn/HZSM-5 and Ga/HZSM-5, while the active component, Zn or Ga, can be lost during the reaction [37]. As a solution, Ga or Zn is inserted into the framework of HZSM-5, but this leads to the decrease in the activity. It is reported that H-Ga (or Zn, Ge)-ZSM-5 [38–41] modified by Pt gives optimal results despite that n-C_4H_{10} is seriously cracked on Pt/HZSM-5 [22,41].

The catalytic performance of Mo/HZSM-5 for the aromatization of n-C_4H_{10} is reported poor [30], but some problems are noticed in the operation conditions: the catalyst was seldom pre-treated before the reaction, the reaction temperature was usually below 823 K and the total reaction time was short. When n-C_4H_{10} converted over supported MoO_3, the bulk molybdenum species were mainly kept as MoO_2 under those conditions [42]. While it is suggested that Mo_2C/HZSM-5 is the active catalyst for the aromatization of CH_4 [43,44] or C_2H_6 [45] although the precursor is MoO_3/HZSM-5. So, it is suspected that Mo_2C/HZSM-5 might be more effective for the aromatization of hydrocarbons than MoO_2/HZSM-5 and that the poor caburization of MoO_3 is responsible for the low aromatization performance of Mo/HZSM-5 as reported in the literature.

To prove this idea, the comparison of the catalytic performance of Mo/HZSM-5 containing different molybdenum species is necessary. But the knowledge in this aspect in literatures is not enough. Thus, the objectives of this work are to investigate the aromatization performance of Mo/HZSM-5 with different molybdenum phases and to explore the possibility to upgrade n-C_4H_{10} using Mo/HZSM-5 catalysts.

2. Experimental

MoO_3/HZSM-5 was prepared by incipient wetness impregnation method. HZSM-5 ($SiO_2/Al_2O_3 = 80$, $S_{BET} = 425\,m^2/g$, CBV 8014G, Zeolyst International) was impregnated with the aqueous solution of ammonia paramolybdenate (A. R.) at room temperature for 24 h, followed by a drying at 393 K for 12 h and a calcination at 773 K in air for another 6 h. The sample of MoO_3/HZSM-5 was pressed, crushed and sieved into granules with the size of 425–600 μm before the reaction test.

The catalytic performance of Mo/HZSM-5 was tested in a fixed bed micro-reactor comprising of a ϕ 13 mm × 3 mm stainless steel tube containing 0.5 g of catalyst. The reactants, 10% (v/v) n-C_4H_{10} (99%, BOC) balanced by He (99.99%, BOC), flowed through the reactor with a rate of 7.5 ml/min controlled by mass flow controllers (Brooks, The Netherlands). In most cases, MoO_3/HZSM-5 was in situ pre-reduced by H_2. After this pre-treatment, the gas was switched from H_2 to He and flushed through the reaction system at lower temperature for enough time, then the temperature of the reactor was increased to and kept at the reaction temperature for 0.5 h before the reactants were introduced into the reaction system.

The analysed products were sampled on line by six-way valves. C_1–C_5 hydrocarbons were analysed by a Varian 3400 CX GC equipped with a 30 m PLOT-Al_2O_3 capillary column, and other heavier hydrocarbons were analysed by a Varian 3400 with a 30 m HP-1 capillary column. In the latter case, the sampler was kept at 513 K, the tube between the outlet of the reactor and the sampler was kept at 473 K. H_2, CO_x, H_2O and coke deposits were not analysed. To calculate the carbon balance, the volume of the effluent was measured by a wet gas flow meter. The conversion of n-C_4H_{10} and the selectivity to the products were expressed by C% and calculated based on the number of hydrocarbons in the effluent analysed by GC.

The X-ray powder diffraction patterns of Mo/HZSM-5 samples were obtained with a Siemens D-5005 diffractometer (2θ mode, Cu Kα Radiation), the scanning step was 0.014°. The nature of the crystalline phases was checked using the XRD patterns in literatures and the database of the Joint Committee on Powder Diffraction Standards (JCPDS). When the reduced or the carburized Mo/HZSM-5 were characterised by XRD ex situ, the catalyst sample was cooled rapidly down to room temperature in He flow after the reaction and passivated by 1% of O_2/N_2 at room temperature for 10–12 h. Then the sample was taken out of the reactor quickly and characterised by XRD immediately.

3. Results

3.1. Effect of the pre-reduction of MoO_3/HZSM-5 on the conversion of n-C_4H_{10}

The relatively weak XRD signals of α-MoC_{1-x} (to be convenient, fcc-molybdenum carbide is labelled as α-MoC_{1-x} in this paper, similarly, hcp-molybdenum carbide is labelled as β-Mo_2C) led us to choose 40 wt.% Mo/HZSM-5 (40 wt.% is for Mo) as the catalyst in order to observe clearly the evolution of the molybdenum phases during the conversion of n-C_4H_{10} [46]. The temperature, where $\Delta G^{\circ}_{\text{reaction}} = 0$, is 643 K for the aromatization of n-C_4H_{10} in thermodynamics [47], but when the temperature was below 773 K, the activity of the 40 wt.% Mo/HZSM-5 ($SiO_2/Al_2O_3 = 80$) catalyst was quite low. To improve the activity, the reaction temperature could be higher, while this would lead to the sublimation of MoO_3 and the destruction of the framework of ZSM-5 by MoO_3 [48]. Separate experiments prove that these side effects are weak on pre-reduced MoO_3/HZSM-5, so the catalyst was pre-reduced by H_2 at relatively lower temperature before the reaction.

MoO_3/HZSM-5 was reduced to MoO_2/HZSM-5 using H_2-TPR method. To avoid the formation of molybdenum metal, the reduction temperature was controlled in the range of 673–773 K and the ramp rate was 10 K/min. The XRD pattern of the pre-reduced sample is shown in Fig. 1. For the fresh MoO_3/HZSM-5 (Fig. 1b), the strong peaks with 2θ at 23.2, 25.6, and 27.2° are typical of MoO_3, the characteristic peaks of HZSM-5 at 23.0, 23.8, and 24.2° are very weak, which is obviously due to the high loading of MoO_3. After the pre-reduction (Fig. 1c), many typical peaks of MoO_3 disappear and the remained MoO_3 peaks are weak, while the peaks due to MoO_2 (25.9, 36.9, 53.4, 60.3, 66.5, and 78.8°, etc.) are observed. It is obvious that the bulk MoO_3 transforms into MoO_2 during the pre-reduction.

The reaction results of n-C_4H_{10} on MoO_3/HZSM-5 and pre-reduced MoO_3/HZSM-5 at 773 K are shown in Fig. 2a and b. An induction period is observed in both cases and the variation of product distribution is similar. For the fresh MoO_3/HZSM-5 (Fig. 2a), the induction period is ∼80 min. During the induction period, the initial selectivities to CH_4 and C_2H_4 are 32 and 24%, respectively, they both decrease quickly with the reaction time, the selectivity to aromatics is as low as 10% at the beginning while increased to ∼30% in the end of the induction period. For the pre-reduced MoO_3/HZSM-5, the induction period is just about

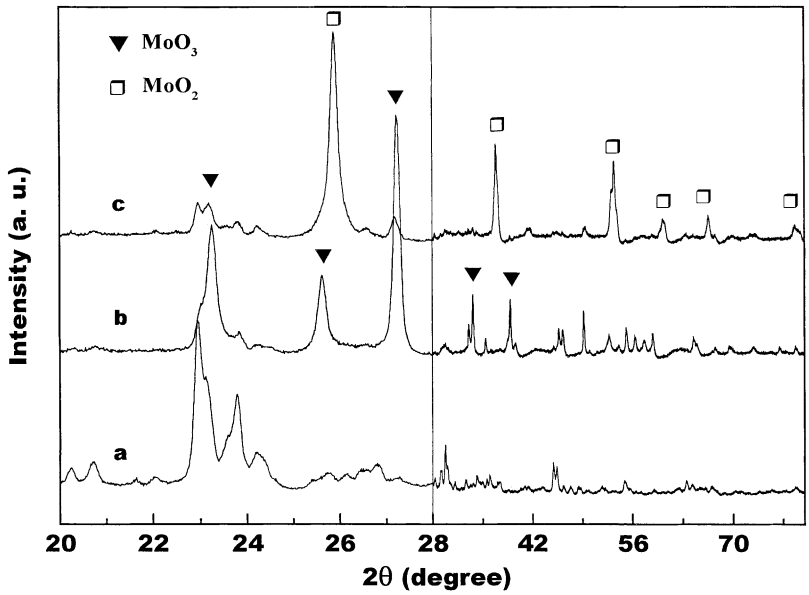

Fig. 1. The XRD patterns of: (a) HZSM-5, (b) MoO_3/HZSM-5, (c) pre-reduced MoO_3/HZSM-5.

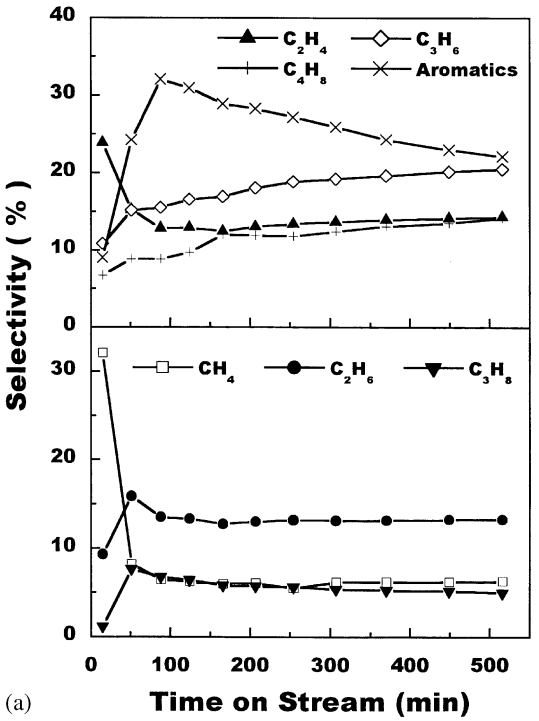

Fig. 2. The variation of product distribution with time on stream during the conversion of *n*-C_4H_{10} at 773 K on: (a) MoO_3/HZSM-5, (b) pre-reduced MoO_3/HZSM-5.

30 min, the initial selectivities to CH_4 and C_2H_4 are 13 and 15%, respectively, while the selectivity to aromatics increases from 25 to 45% during the induction period.

These demonstrate that the variation of the selectivity to CH_4 (or C_2H_4 and aromatics) with the reaction time during the induction period (Fig. 2a and b) is similar to the variation of the selectivity to CH_4 (or C_2H_4 and aromatics) caused by the pre-reduction of MoO_3/HZSM-5 as shown by the initial selectivities to the products in Fig. 2a and b. Because the bulk molybdenum species of MoO_3/HZSM-5 changes into MoO_2 after the pre-reduction (Fig. 1) and the bulk MoO_2 are hardly further carburized at 773 K (cf. Fig. 6a), it is reasonable to conclude that the change in MoO_x of Mo/HZSM-5 during the induction period is the reduction of MoO_3 to MoO_2 and that the variation of the product distribution is partially related to the consumption of oxygen in MoO_3.

The rather low initial selectivity to aromatics for MoO_3/HZSM-5 and the increase in the selectivity to aromatics with the reduction of MoO_3 to MoO_2 (Fig. 2a) indicate that the aromatization performance of MoO_3/HZSM-5 is poor and lower than that of MoO_2/HZSM-5. This could be explained by the production of CO_x from the deep oxidation of *n*-C_4H_{10}, as indicated by the consumption of oxygen and the low carbon balance (50–70%, which is not shown here) during the induction period, and the serious cracking reaction as suggested by the decreased selectivities to CH_4, C_2H_4 and C_2H_6 with the consumption of oxygen in the Mo/HZSM-5.

3.2. Conversion of n-C_4H_{10} at different temperatures on pre-reduced MoO_3/HZSM-5

Fig. 3 presents the conversion of *n*-C_4H_{10} as the function of temperature and time on stream. The initial conversion increases to 100% when the reaction temperature rises from 773 up to 893 K. The initial conversion in the case of 773 or 813 K is relatively higher, then decreased gradually to a stable value. While for the case of 853 K, no stable conversion but a maximum conversion is observed, the time for the maximum conversion is at about 5 h at 853 K. The conversion at 893 K (or 933 and 973 K) reaches its maximum (∼100%) at the starting point and keeps there

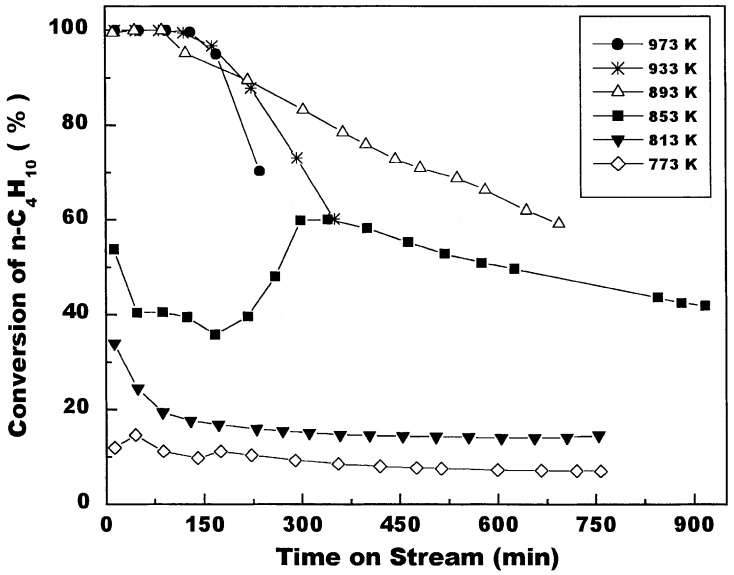

Fig. 3. The variation of the conversion of n-C_4H_{10} with time on stream over pre-reduced MoO_3/HZSM-5 at different reaction temperatures.

for a period of time, then the conversion decreases, the higher the reaction temperature, the faster the conversion decreases.

For the reaction at 853 K, the variation of conversion with reaction time is quite different. In the first 50 min, the conversion decreases from 57 to 40% and the conversion changes little within the next 2 h. But the conversion of n-C_4H_{10} is surprisingly increased from 40% at 170 min to 60% at 300 min and then decreases gradually again.

The carbon balance of the reaction at different temperatures is shown in Fig. 4. The figure discloses that

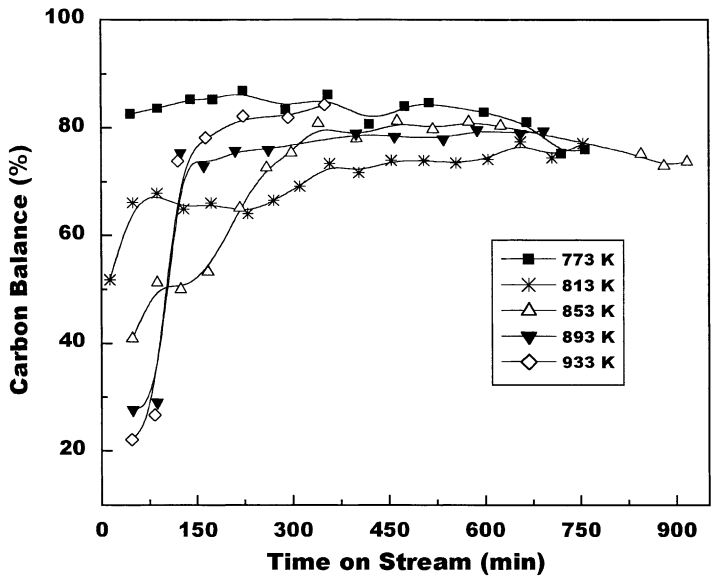

Fig. 4. The carbon balance during the conversion of n-C_4H_{10} over pre-reduced MoO_3/HZSM-5 at different reaction temperatures.

the initial carbon balance is lower for the reaction temperatures above 813 K but increases with the reaction time and reaches 70–85% at the late stage. The difference in the carbon balance of the reaction at different temperatures mainly appears at the early stage, the starting carbon balance is ∼80% at 773 K, while it decreases to ∼50% at 813 K, 40% at 853 K, lower than 30% at 893 or 933 K.

The variation of the product distribution in the effluent with temperature and time on stream is shown in Figs. 2b and 5a-e. The hydrocarbon products in the gas phase are mainly CH_4, C_2H_6, C_2H_4, C_3H_6, C_3H_8, butylene and C_6–C_{10} aromatics including benzene, toluene, xylene and naphthalene. The selectivities to *i*-butane and C_5 hydrocarbons are lower than 5% in all cases, which are not shown in the figures.

The variation of the product distribution in the effluent at 853 K (Fig. 5b) shows that there are at least three stages. The first is in the first 90 min. The initial selectivities to C_6H_6, CH_4 and C_2H_6 are all close to 25%. The selectivity to C_2H_4 (or C_2H_6 and aromatics) decreases with time, while the selectivity to CH_4 reaches it maximum (28%) at 90 min, the selectivity to butylene also increases. The second is in the next 80 min, the selectivities to aromatics, C_2H_4 and C_2H_6 are stable, while the selectivity to butylene is increased further to a maximum (15%). The third period is from 170 to 300 min, the selectivities to aromatics, C_2H_4 and C_3H_6 rises up to 35, 13 and 12%, respectively, while the selectivities to butylene, CH_4 and C_2H_6 decrease to ∼10, 15 and 15%, respectively. When the reaction proceeds further, the selectivity to aromatics is gradually decreased, which is accompanied by a slow increase in the selectivity to butylene, while the selectivity to the other products is stable.

The variation of the product distribution of the reaction at 893 K (Fig. 5c) is similar to that at 853 K, but the product distribution changes a lot. The first period is ∼50 min and the initial selectivities to CH_4, C_2H_6, C_2H_4 and aromatics are 51, 2.5, 36 and 10.5%, respectively. In the second period, i.e. ∼50 to ∼95 min, CH_4 is the sole hydrocarbon product in the gas. After 95 min, the selectivity to C_2H_4 (or C_2H_6, C_3H_6 and butylene) increases quickly from zero to its stable maximum. While the selectivity to aromatics is gradually decreased after it reaches its maximum (∼42%) within 50 min and the selectivity to CH_4 is simultaneously decreased from 100% to a stable minimum of ∼25%.

The cases at 813 K (Fig. 5a), 933 K (Fig. 5d) and 973 K (Fig. 5e), can be regarded as the special cases of those at 853 and 893 K, i.e. the variation of the product distribution at 813 K is similar to that in the first two stages at 853 or 893 K, the variation of the reaction at 933 or 973 K is similar to the latter two stages at 853 or 893 K. But the periods of the first two stages become shorter at higher reaction temperature (Fig. 5a–e), the rising reaction temperature also leads to the increase in the selectivity to CH_4 and the decrease in the selectivities to some other higher hydrocarbons as for the first two stages.

The XRD patterns of the catalysts after the conversion of *n*-C_4H_{10} at different temperatures are shown in Fig. 6. After the reaction at 773 K for ∼760 min (Fig. 6a), only the strong peaks due to MoO_2 are observed, the rest peaks are ascribed to ZSM-5.

For the Mo/HZSM-5 sample after the conversion of *n*-C_4H_{10} at 853 K (Fig. 6c), no XRD peaks of MoO_2 are observed, the broad peaks at 36.8, 41.2, 61.6, and 73.8° are due to α-MoC_{1-x}. The peak at 36.8° is much higher than that at 41.2°, which might reflect the low specific surface area of the formed α-MoC_{1-x} [49]. Compare the XRD pattern of Fig. 6b to that of Fig. 6c, the appearance of peaks at 41.3, 61.6 and 74.0° in Fig. 6b suggests the formation of α-MoC_{1-x} in the case of 813 K.

The XRD pattern of the Mo/HZSM-5 sample after the reaction at 893 K (Fig. 6d) is similar to that in the case of 853 K, but another small broad peak appears at 34.3° in Fig. 6d. For the case at 933 K (Fig. 6e), the peak at 34.3° becomes quite clear and the typical broad peak of α-MoC_{1-x} at ∼41° in Fig. 6d is not observed but a broad peak appears at 39.3°. The intensity of the peak at 39.3° is a little weaker than that of the peak at 37.0°. The XRD pattern of the sample treated by *n*-C_4H_{10} at 973 K for 237 min (Fig. 6f) is similar to that in Fig. 6e, the peaks at 34.3, 39.3, 61.6 and 74.4° are all quite sharp and the intensity of the peak at 39.3° is stronger than that of the peak at 37.4°. The three peaks with 2θ at 34.3, 37.3 and 39.5° are typical of β-Mo_2C. Based on this assignment and the comparison of the figures (Fig. 6d–f), β-Mo_2C begins to be produced at 893 K. For the sample after

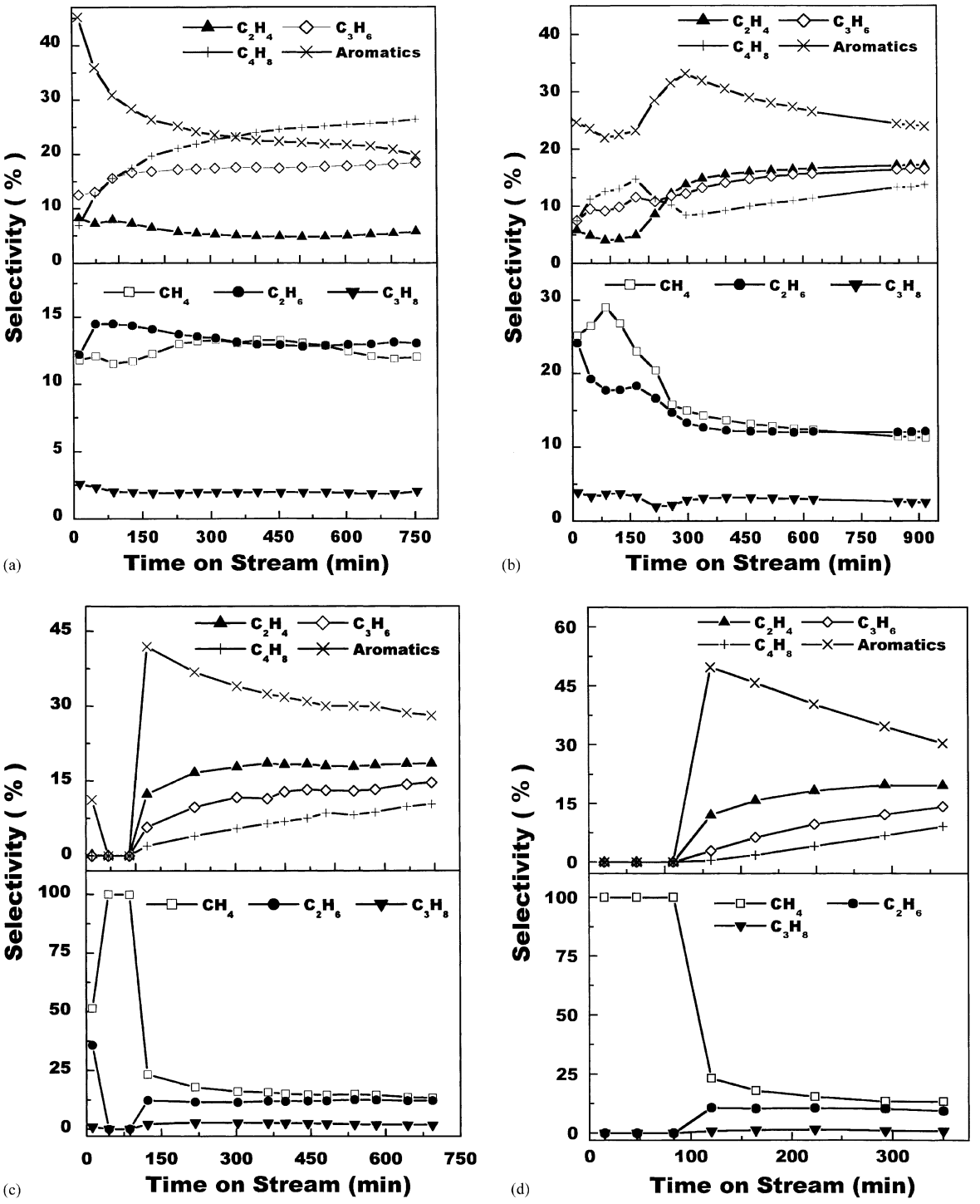

Fig. 5. The variation of the product distribution with time on stream during the conversion of *n*-C_4H_{10} at: (a) 813, (b) 853, (c) 893, (d) 933 and (e) 973 K on pre-reduced MoO_3/HZSM-5.

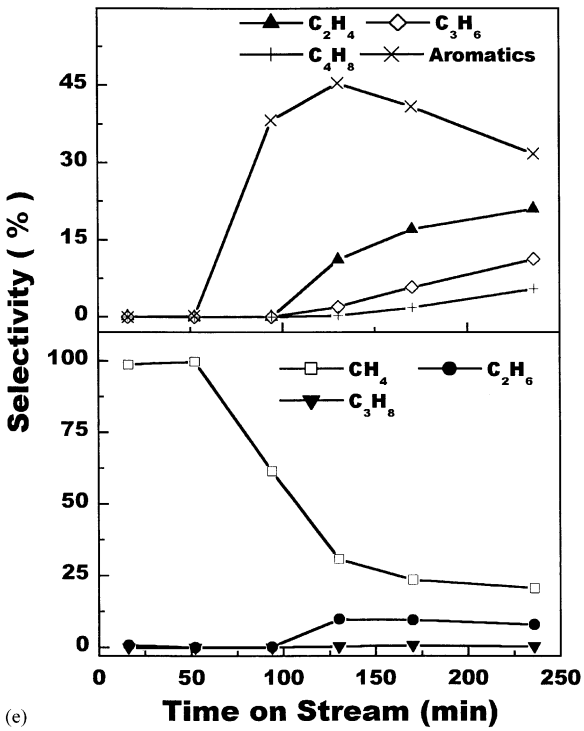

Fig. 5. (*Continued*).

the reaction at 933 K, although the typical peak of α-MoC_{1-x} at ∼41° is not observed, the existence of α-MoC_{1-x} can not be excluded.

The peaks of HZSM-5 at 22.9, 23.8 and 24.2° are observed in all the XRD patterns (Fig. 6a–f), which indicates that the framework of ZSM-5 is stable in the temperature range of 773–973 K. Nevertheless, the disappearance of the shoulder at ∼23.1° in Fig. 6d and e suggests that there might be some changes in the morphology of ZSM-5 after the conversion of *n*-C_4H_{10} proceeded for enough time above 853 K [50]. Because the doublets at ∼24.2 and ∼29° are weak and obscure, it is assumed that orthorhombic ZSM-5 and monoclinic ZSM-5 coexist [50,51].

Fig. 7 gives the XRD patterns of the Mo/HZSM-5 samples for different time at 853 K. After the reaction of *n*-C_4H_{10} proceeds for 35 min (Fig. 7a), the peaks due to MoO_3 at 23.2 and 27.2° (Fig. 1c) disappear and only XRD peaks of MoO_2 are observed. After 70 min on stream (Fig. 7b), the bulk molybdenum oxide is still maintained as MoO_2. When the reaction time is prolonged to 120 min (Fig. 7c), the peaks of MoO_2 are still strong, but the peaks of α-MoC_{1-x} become distinct. After 238 min on stream (Fig. 7d

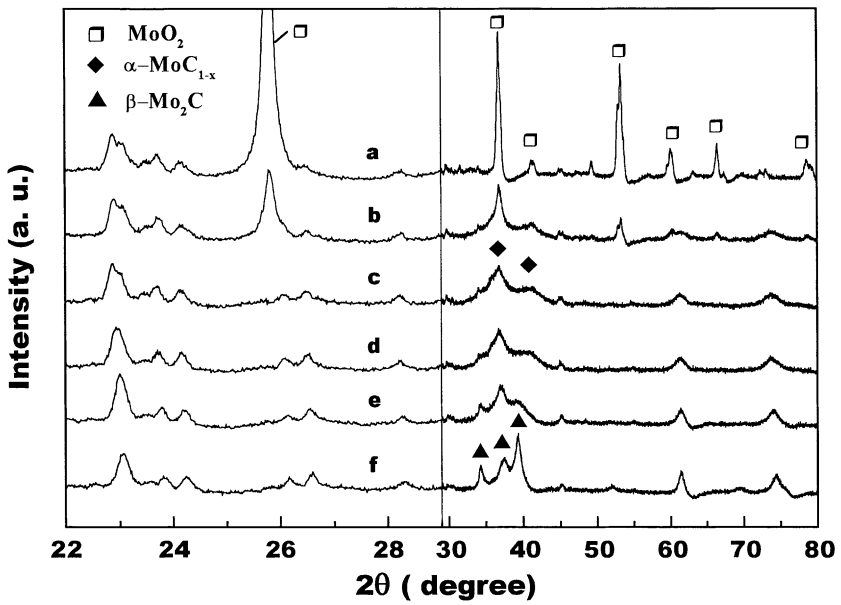

Fig. 6. The XRD patterns of Mo/HZSM-5 samples after the conversion of *n*-C_4H_{10} at: (a) 773 K for 758 min, (b) 813 K for 754 min, (c) 853 K for 922 min, (d) 893 K for 693 min, (e) 933 K for 352 min and (f) 973 K for 237 min.

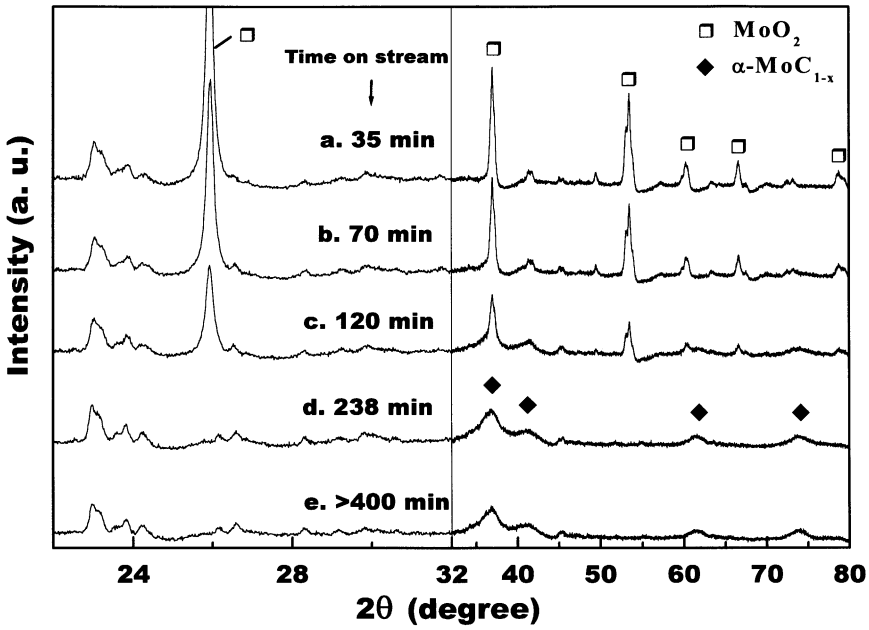

Fig. 7. The XRD patterns of Mo/HZSM-5 samples during the conversion of n-C_4H_{10} at 853 K for different reaction time.

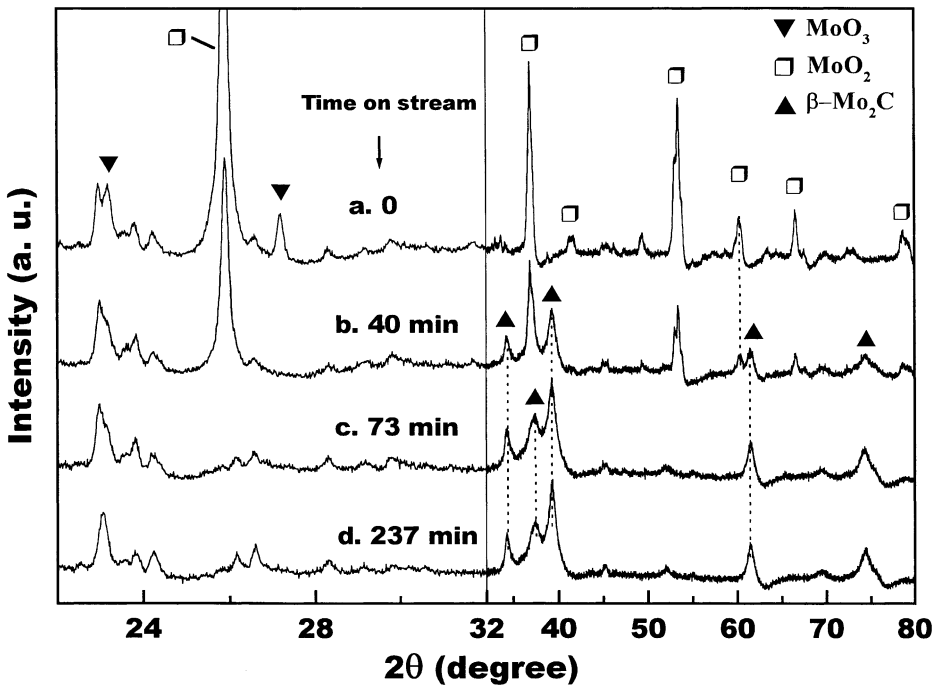

Fig. 8. The XRD profiles of Mo/HZSM-5 samples during the conversion of n-C_4H_{10} at 973 K for different reaction time.

Table 1
The conversion of n-C_4H_{10} over pretreated 40 wt.%Mo/HZSM-5 at different conditions

	773 K		813 K	
	Pre-reduced	Pre-carburized	Pre-reduced	Pre-carburized
Conversion (%)	7.4	16.2	24.4	51.0
Product distribution (%)				
CH_4	6.1	6.6	12.2	10.3
C_2H_6	10.5	10.6	14.6	12.0
C_2H_4	9.5	10.5	7.3	11.7
C_3H_6	1.8	3.4	2.3	3.5
C_3H_8	19.2	18.3	13.3	14.0
i-C_4H_{10}	1.5	3.6	0.9	2.1
C_4H_8	25.5	22.2	12.5	11.8
C_5	0.9	0.6	0.9	0.5
Aromatics	24.8	24.0	35.9	34.3
Aromatics distribution (%)				
Benzene	36.0	42.8	42.3	45.2
Toluene	43.0	39.4	37.2	36.3
C_{8+}	21.0	17.7	20.5	18.4

and e), all the peaks of molybdenum species are due to α-MoC_{1-x}.

Fig. 8 shows the XRD patterns of the Mo/HZSM-5 samples for different time at 973 K. When the reaction proceeds only for 40 min (Fig. 8b), the peaks of MoO_3 disappear and the peaks of MoO_2 decrease dramatically. Moreover, the peaks of β-Mo_2C are observed and the intensity of the peak at 34.3 or 39.3° is quite strong. After 73 min on stream (Fig. 8c and d), the peaks of the β-Mo_2C become stronger, which is accompanied by the disappearance of the peaks of MoO_2.

3.3. Catalytic performances of pre-reduced MoO_3/HZSM-5 and of pre-carburized MoO_3/sHZSM-5 for the conversion of n-butane

The catalytic performances of MoO_2/HZSM-5 and of fresh Mo_2C/HZSM-5 are compared and the results are listed in Table 1, the procedure for the carburization of MoO_3/HZSM-5 is published elsewhere [46]. Whether the reaction takes place at 773 or 813 K, the distribution of the products for the two catalysts is nearly the same, while the conversion of n-C_4H_{10} for the pre-carburized Mo/HZSM-5 is much higher than that for the pre-reduced Mo/HZSM-5.

4. Discussion

4.1. Evolution of the molybdenum phases on Mo/HZSM-5

The XRD results in Fig. 6 disclose that the carburization of the bulk MoO_2 is difficult although MoO_3 is readily reduced by n-C_4H_{10} into MoO_2 at 773 K. Molybdenum carbide can be produced above 813 K, α-MoC_{1-x} and β-Mo_2C co-exist between 853 and 933 K, while the bulk molybdenum species exist mainly as β-Mo_2C at 973 K. The XRD results in Figs. 7 and 8 further show that MoO_2 coexists with Mo_2C before MoO_3 changes into Mo_2C.

In the literature, α-MoC_{1-x} is usually prepared from MoO_3 by H_2/C_nH_{2n+2}-TPR method [25,26, 52,53]. MoO_3 transforms into $MoO_xC_yH_z$ in H_2/C_nH_{2n+2} ($x \geq 2$) at 623 K and $MoO_xC_yH_z$ will be further carburized to α-MoC_{1-x} at high temperatures. The whole process from MoO_3 to α-MoC_{1-x} is topotactic [54–57] and the formation of $MoO_xC_yH_z$ is believed to be the key step to form α-MoC_{1-x} [57]. While the present results show that α-MoC_{1-x} can be produced directly from the reaction between n-C_4H_{10} and MoO_3/HZSM-5 through MoO_2/HZSM-5. Because the process from MoO_3 to MoO_2 is non-topotactic [53], the present results

prove actually that α-MoC_{1-x} and β-Mo_2C can be both prepared from the carburization of MoO_3 by hydrocarbons in a non-topotactic way. This conclusion is also confirmed by the SEM results, which are not shown here.

It should be pointed out that when unsupported MoO_3 is treated with *n*-C_4H_{10} by TPR method with the ramp of 3 K/min, in situ XRD results show that MoO_2 is the sole bulk molybdenum species below 893 K, no α-MoC_{1-x} but β-Mo_2C is observed when the reaction temperature is further increased up to 993 K. These results are different from the case of 40 wt.% Mo/HZSM-5. It is unclear whether this is due to the different temperature programs (the reaction temperature is kept stationary at 853 or 973 K in the case of 40 wt.%Mo/HZSM-5, while TPR is used for the in situ characterization of unsupported MoO_3) or HZSM-5 plays a role during the formation of α-MoC_{1-x}. The effect of support on the structure of molybdenum carbide prepared from the carburization of MoO_3 by hydrocarbons was also reported in literature [57].

4.2. Catalytic performance of Mo/HZSM-5 with different molybdenum phases for the conversion of n-C_4H_{10}

For the case at 853 K (Fig. 5b), the selectivities to aromatics and some other products vary monotonously with the reaction time between 170 and ∼300 min. The corresponding bulk molybdenum species on Mo/HZSM-5 change into Mo_2C at 240 min for 853 K (Fig. 7d, e). After the reaction proceeds for 50 min at 973 K (Fig. 5e), the variation of the selectivity to aromatics is similar to that between 170 and 300 min at 853 K, the bulk molybdenum species are molybdenum carbide (Fig. 8c and d). In the first 50 min at 973 K, the distribution of the products in the effluent changes little (100% CH_4), the XRD results show that Mo_2C coexists with MoO_2. Similarly, for the case at 853 K, when Mo_2C and MoO_2 coexist between 100 and 170 min (Fig. 7b–e), the variation of the selectivities to aromatics and some other products changes a little (Fig. 5b). This similarity is also observed after the induction period in the case of 773 K, the whole case at 813 K and in the first 70 min in the case at 853 K, the corresponding molybdenum phases on Mo/HZSM-5 are MoO_2.

The correlation of the variation of the product distribution with the molybdenum phases at different temperatures shows clearly that although the molybdenum loading on 40 wt.% Mo/HZSM-5 is rather high, the reaction results are still closely related to the bulk molybdenum species. This relationship provides us the base to infer the evolution of the bulk molybdenum species from the extrapolation of the selectivity to product versus reaction time curve during the reaction at 893 or 933 K, which was not extensively characterised by XRD. In detail, the time for the disappearance of bulk MoO_x on 40 wt.% Mo/HZSM-5 should be at ∼170 min for the case at 853 K (Fig. 5b), ∼90 min for 893 K (Fig. 5c), ∼80 min for 933 K (Fig. 5d) and ∼50 min for 973 K (Fig. 5e). The time for MoO_2 to co-exist with Mo_2C is between ∼100 and 170 min for 853 K (Fig. 5b), 50 to 90 min for 893 K (Fig. 5c), within the first 80 min for 933 K (Fig. 5d) and in the first 50 min for 973 K (Fig. 5e).

For the period when the bulk molybdenum species are mainly MoO_2, the bulk molybdenum species changes little, the consumption of the oxygen in the catalyst should be limited and so the amount of CO_x in the products should also be small. Moreover, the carbon balance (Fig. 4) is always lower than 100%. These points hint that the decrease in the conversion (Fig. 3) or the selectivity to aromatics (Figs. 2b, 5b, c) with the reaction time might be caused by the coke deposits. The stability of MoO_2 and the continuous variation of the product distribution or the conversion with time on stream suggest that MoO_2/HZSM-5 could be the catalyst for the aromatization of *n*-C_4H_{10} below 813 K. But the selectivity to aromatics decreased quickly (e.g. the initial selectivity decreases from 45% at 773 K to 25% at 853 K) while the selectivity to the cracking products (CH_4 and C_2H_6) increases rapidly with temperature when the temperature is higher than 813 K. The carbon balance in this period also decreases with the rising reaction temperature (Fig. 4). These demonstrate that cracking, coke deposition and/or deep oxidation of *n*-C_4H_{10} are serious, which are obviously originated from the instability of MoO_x above 813 K. Thus, MoO_2/HZSM-5 is not suitable to catalyse the aromatization of *n*-C_4H_{10} above 813 K.

When MoO_2 coexists with Mo_2C, the conversion of *n*-C_4H_{10} with time on stream is relatively stable (Fig. 5a–c). While the selectivities to CH_4 and

aromatics are 13% and 20–25% for 813 K (Fig. 5b, at the late stage), 20–30% and 20–25% for 853 K (Fig. 5c), 100 and ∼0% for 893 K (Fig. 5d), respectively. Obviously, the selectivity to the complete cracking product, CH_4, is high at high reaction temperature. But the selectivity to CH_4 decreases when bulk MoO_2 is carburized to Mo_2C at 853 K (between 90 and 170 min, Fig. 5c). These suggest that the existence of oxygen in Mo/HZSM-5 and high reaction temperature promote the cracking of n-C_4H_{10}. Because the carburization of MoO_2 is the process for the reduction of MoO_2 and the substitution of the oxygen in MoO_2 by carbon, so some other carbon must exist as CO_x and/or coke deposits as evidenced by the low carbon balance (Fig. 4) besides the hydrocarbon products when MoO_2 is transformed into molybdenum carbide.

Contrasted with the conversion of n-C_4H_{10} on MoO_2/HZSM-5 or (Mo_2C + MoO_2)/HZM-5, the conversion of n-C_4H_{10} on Mo_2C/HZSM-5 is quite different. Although coke deposition is serious, as evidenced by 70–80% of carbon balance (Fig. 4), the reaction proceeds with 30–40% of selectivity to aromatics at 773–973 K on Mo_2C/HZSM-5 (Figs. 2b and 5b-e). Moreover, for the conversion of n-C_4H_{10} on Mo_2C/HZSM-5, the maximum selectivity to aromatics is 24% at 773 K, ∼34% at 813 K (Table 1), 33% at 853 K and 45% at 893 or 973 K (Fig. 5b–e). These indicate that the higher reaction temperature is helpful to the aromatization reaction when n-C_4H_{10} conversed on Mo_2C/HZSM-5 (Fig. 3). This analysis and the results in Table 1 lead us to the conclusion that Mo_2C/HZSM-5 is a better catalyst than MoO_2/HZSM-5 or (MoO_2 + Mo_2C)/HZSM-5 for the aromatization of n-C_4H_{10}.

It is noted that the maximum selectivity to aromatics appears at ∼300 min for the case at 853 K, 150 min for 893 K, 125 min for 933 K and 125 min for 973 K (Fig. 5b–e). The time is longer than the corresponding time when bulk MoO_x evolves into Mo_2C. So there might be some other factors affecting the production of aromatics apart from the molybdenum species. Similar phenomena are observed in the aromatization of CH_4 over Mo/HZSM-5 catalyst [58], it was suggested that suitable amount of coke on Mo_2C/HZSM-5 is favourable to the production of aromatics.

Last, it must be emphasized that the idea to magnify the XRD signals of the molybdenum species led us to use 40 wt.% Mo/HZSM-5 as the sample in this work. In fact, the Mo/HZSM-5 sample with lower molybdenum loading on which the molybdenum phases detectable by XRD gives the same results. The unique conversion versus reaction time curve at 853 K (Fig. 3) was also observed on the Mo/HZSM-5 catalysts with the molybdenum loading of 3–20 wt.% when the reaction took place at 813 K. Raman spectroscopy proved that even for 3 wt.%Mo/HZSM-5 (the sample is the mixture of MoO_3 and HZSM-5), crystal MoO_3 was still observed on the catalyst when the heating temperature is lower than 823 K [59]. The characterization of Mo/HZSM-5 by XPS also showed that there is a period for the reduction and carburization of the molybdenum oxide when CH_4 [43] or C_2H_6 [45] aromatized over 2–4 wt.% Mo/HZSM-5. So although the coke deposits and CO_x were not detected, the variation of the conversion versus reaction time curve and/or the selectivity to aromatics versus reaction time curve in this paper is also typical and can reflect the carburization process of MoO_3 of the MoO_3/HZSM-5 with molybdenum loading higher than 3 wt.%.

5. Conclusions

During the conversion of n-C_4H_{10} over MoO_3/HZSM-5, MoO_3 transforms directly into α-MoC_{1-x} or β-Mo_2C through the intermediate of MoO_2. The structure of the produced molybdenum carbide can be controlled by the reaction conditions, the formation of β-Mo_2C requires a higher reaction temperature (>893 K).

The reduction and carburization of MoO_x during the conversion of n-C_4H_{10} over MoO_3/HZSM-5 leads to the formation of Mo/HZSM-5 with different molybdenum phases: MoO_3/HZSM-5, MoO_2/HZSM-5, (MoO_2 + Mo_2C)/HZSM-5 and Mo_2C/HZSM-5. Aromatization of n-C_4H_{10} can take place on all these samples, but the efficiency is different. MoO_3 is readily reduced by n-C_4H_{10} to MoO_2, while n-C_4H_{10} is simultaneously oxidised to CO_x and cracked to C_1–C_3 hydrocarbons. When the temperatures is lower than 813 K, the conversion of n-C_4H_{10} for the fresh Mo_2C/HZSM-5 is much higher than that for MoO_2/HZSM-5 catalyst in spite of the similar product distribution. MoO_2 is unstable in n-C_4H_{10} and carburized into Mo_2C above 813 K, the carburization

process is accompanied by the serious coke deposit, the deep oxidation and the cracking of n-C_4H_{10}. Mo_2C/HZSM-5 can well catalyse the aromatization of n-C_4H_{10} in the temperature range of 773–973 K although the catalyst deactivates quickly at high temperatures. So, Mo_2C/HZSM-5 has better aromatization performance than MoO_2/HZSM-5.

Acknowledgements

This work is financially supported by the British Council in Beijing, China (Project PEK/0992/297) and the State Key Project of the Ministry of Science and Technology (Grant 19999022407), Peoples Republic of China. The authors would also like to thank Mr. B. Tonney, Dr. J.R. Anderson, and Dr. C. Bouchy in LCIC for their kind help and constructive suggestions.

References

[1] J. Happel, H. Blanck, T.D. Hamill, Ind. Eng. Chem. Fundam. 5 (1966) 289.
[2] G.A. Stepanov, A.L. Tsailingold, V.A. Levin, F.S. Pilipenko, Stud. Surf. Sci. Catal. 7 (1981) 1293.
[3] M.A. Chaar, D. Patel, M.C. Kung, H.H. Kung, J. Catal. 105 (1987) 483.
[4] D. Patel, P.J. Andersen, H.H. Kung, J. Catal. 125 (1990) 132.
[5] W.R. McDondald, A.D. McIntyre, US Patent 3119111 (1964).
[6] S.T. Sie, Handbook of Heterogeneous Catalysis, Vol. 4, VCH, Weinheim, 1997, p. 2014.
[7] Anno., Hydrocarbon Processing 61 (9) (1982) 170.
[8] E. Baburek, J. Nováková, Appl. Catal. A 190 (2000) 241.
[9] P. Canizares, A. Lucas, F. Dorado, A. Duran, I. Asencio, Appl. Catal. A 169 (1998) 137.
[10] P. Canizares, A. Lucas, J.L. Valverde, F. Dorado, Ind. Eng. Chem. Res. 37 (1998) 2592.
[11] R. Byggningsacka, N. Kumar, L.E. Lindfors, Catal. Lett. 55 (1998) 173.
[12] G.D. Pirngruger, K. Seshan, J.A. Lercher, J. Catal. 186 (1999) 188.
[13] G.D. Pirngruger, K. Seshan, J.A. Lercher, J. Catal. 190 (1999) 396.
[14] M.M. Agudelo, T. Romero, J. Guaregua, M. Gonzalez, US Patent 5416052 (1995).
[15] V.K. Shum, US Patent 4962266 (1990).
[16] Ch.-L. O'Young, J.E. Browne, J.F. Matteo, R.A. Sawicki, J. Hazen, US Patent 5198597 (1993).
[17] G.D. Pirngruber, O.P.E. Zinck-Stagno, K. Seshan, J.A. Lercher, J. Catal. 190 (2000) 374.
[18] Y. Ono, Catal. Rev. Sci. Eng. 34 (1992) 179.
[19] M. Guisnet, N.S. Gnep, F. Alario, Appl. Catal. A 89 (1992) 1.
[20] N. Kumar, L.E. Lindfors, R. Byggningsbacka, Appl. Catal. A 139 (1996) 189.
[21] N. Kumar, L.E. Lindfors, Appl. Catal. A 147 (1996) 175.
[22] W.J.H. Dehertog, G.F. Fromen, Appl. Catal. A 189 (1999) 63.
[23] R.L. Levy, M. Boudart, Science 181 (1973) 547.
[24] S.T. Oyama, Catal. Today 15 (1992) 179.
[25] J.G. Chen, Chem. Rev. 96 (1996) 1477.
[26] S.T. Oyama, et al., The Chemistry of Transition Metal Carbides and Nitrides, Blackie, Glasgow, 1996.
[27] J.G. Chen, J. Eng Jr., S.P. Kelty, Catal. Today 43 (1998) 147.
[28] J.G. Chen, B. Fruhberger, J. Eng Jr., B.E. Bent, J. Mol. Catal. A 285 (1998) 31.
[29] M.K. Neylon, S. Choi, H. Kwon, K.E. Curry, L.T. Thompson, Appl. Catal. A 183 (1999) 253.
[30] I.M. Harris, J. Dwyer, A.A. Garforth, C.H. Mcateer, W.J. Ball, Stud. Surf. Sci. Catal. 47 (1989) 271.
[31] T. Yahsima, S. Ejiri, K. Kato, M.M. Ishaq, M. Tanigawa, T. Komatsu, S. Namba, Stud. Surf. Sci. Catal. 447 (1996) 100.
[32] N. Kumar, R. Byggningsbacka, L.E. Lindfors, React. Kinet. Catal. Lett. 61 (1997) 297.
[33] P.C. Doolan, P. Pujado, Hydrocarbon Process 68 (1989) 72.
[34] P. Fejes, J. Halasz, I. Kiricsi, Z. Kele, G. Tasi, E. Derouane, K. Dooley, J.N. Armor, Stud. Surf. Sci. Catal. 75 (1993) 421.
[35] T. Inui, Y. Ishihara, K. Kawashi, H. Matsuda, Stud. Surf. Sci. Catal. 49 (1989) 1183.
[36] G. Giannetto, A. Montes, N.S. Gnep, A. Fluorentino, P. Cartaud, M. Guisnet, J. Catal. 145 (1994) 86.
[37] Y.F. Chu, A.W. Chester, US Patent 4392989 (1983) to Mobil Oil Corp.
[38] T. Inui, Stud. Surf. Sci. Catal. 44 (1989) 189.
[39] E.S. Shpiro, D.P. Shevchenko, R.V. Dmitriev, O.P. Tkachenko, K.M. Minachev, Appl. Catal. A 107 (1994) 165.
[40] A. Matsuoka, J.B. Kim, T. Inui, Micro. Meso. Mater. 35/36 (2000) 89.
[41] T. Komatsu, M. Mesuda, T. Yashima, Appl. Catal. A 194 (2000) 333.
[42] M.E. Harlin, L.B. Backman, A.O.I. Krause, O.J.T. Jylha, J. Catal. 183 (1999) 300.
[43] F. Solymosi, A. Szöke, J. Cserényi, Catal. Lett. 39 (1996) 157.
[44] D. Wang, J.H. Lunsford, M.P. Rosynek, J. Catal. 169 (1997) 347.
[45] F. Solymosi, A. Szöke, Appl. Catal. A 166 (1998) 225.
[46] S. Yuan, S.B. Derouane-Abd Hamid, Y. Li, P. Ying, Q. Xin, E.G. Derouane, C. Li, J. Mol. Catal. A, in press.
[47] G.V. Samsonv, Oxide Handbook, IFI/Plenum Press, New york 1973, p. 216.
[48] W. Liu, Y. Xu, J. Qiu, J. Mol. Catal. A 120 (1997) 257.
[49] J.S. Lee, L. Volpe, F.H. Ribeiro, M. Boudart, J. Catal. 112 (1988) 44.
[50] H. Nakamoto, H. Takahashi, Chem. Lett. (1981) 169.
[51] E.L. Wu, S.L. Lawton, D.H. Olson, A.C. Rohrman Jr., G.T. Kokotallo, J. Phys. Chem. 83 (1979) 2777.
[52] S.Z. Li, W.B. Kim, J.S. Lee, Chem. Mater. 10 (1998) 1853.

[53] L. Volpe, M. Boudart, J. Sol. State Chem. 59 (1985) 332.
[54] C. Pham-Huu, P. Del Gallo, E. Peschiera, M.J. Ledoux, Appl. Catal. A 132 (1995) 77.
[55] P. Del Gallo, G. Meunier, C. Pham-Huu, C. Crouzet, M.J. Ledoux, Ind. Eng. Chem. Res. 36 (1997) 4166.
[56] P. Delporte, F. Meunier, C.P. Pham-Huu, P. Vennegues, M.J. Ledoux, J. Guille, Catal. Today 23 (1995) 251.
[57] C. Bouchy, I. Schmidt, J.R. Anderson, C.J.H. Jacobsen, E. Derouane, D.A.H. Shariafah Bee, J. Mol. Catal. A 163 (2000) 283.
[58] Y. Lu, PhD dissertation, Dalian Institute of Chemical Physics, China, 1999.
[59] W. Li, G.D. Meitzner, R.W. Borry III, E. Iglesia, J. Catal. 191 (2000) 373.